Research Article | Vol. 24, No. 20 | 3 Oct 2016 | OPTICS EXPRESS 22943

Optics EXPRESS

Broadband high birefringence and polarizing hollow core antiresonant fibers

SEYEDMOHAMMAD ABOKHAMIS MOUSAVI,* SEYED REZA SANDOGHCHI, DAVID J. RICHARDSON, AND FRANCESCO POLETTI

Optoelectronics Research Centre University of Southampton, SO17 1BJ, UK
sam1e12@soton.ac.uk

Abstract: We systematically study different approaches to introduce high birefringence and high polarization extinction ratio in hollow core antiresonant fibers. Having shown the ineffectiveness of elliptical cores to induce large birefringence in hollow core fibers, we focus on designing and optimizing polarization maintaining Hollow Core Nested Antiresonant Nodeless Fibers (HC-NANF). In a first approach, we create and exploit anti-crossings with glass modes at different wavelengths for the two polarizations. We show that suitable low loss high birefringence regions can be obtained by appropriately modifying the thickness of tubes along one direction while leaving the tubes in the orthogonal direction unchanged and in antiresonance. Using this concept, we propose a new birefringent NANF design providing low loss (~40dB/km) and high birefringence (>10^{-4}) over a record bandwidth of ~550nm, and discuss how bandwidth can be traded off to further reduce the loss to a few dB/km. Finally, we propose a polarization mode-stripping technique in the birefringent NANF. As a demonstration, we propose a polarizing birefringent NANF design that can achieve orthogonal polarization loss ratios as large as 30dB over the C-band while eliminating any undesirable polarization coupling effect thereby resulting in a single polarization output in a hollow core fiber regardless of the input polarization state.

OCIS codes: (060.2310) Fiber optics; (060.2400) Fiber properties; (060.4005) Microstructured fibers; (060.2420) Fibers, polarization-maintaining.

References and links

1. M. A. Terrel, M. J. F. Digonnet, and S. Fan, "Resonant fiber optic gyroscope using an air-core fiber," J. Lightwave Technol. **30**(7), 931–937 (2012).
2. G. Epple, K. S. Kleinbach, T. G. Euser, N. Y. Joly, T. Pfau, P. S. J. Russell, and R. Löw, "Rydberg atoms in hollow-core photonic crystal fibres," Nat. Commun. **5**, 4132 (2014).
3. A. D. Slepkov, A. R. Bhagwat, V. Venkataraman, P. Londero, and A. L. Gaeta, "Spectroscopy of Rb atoms in hollow-core fibers," Phys. Rev. A **81**(5), 053825 (2010).
4. X. Peng and L. Dong, "Fundamental-mode operation in polarization-maintaining ytterbium-doped fiber with an effective area of 1400 μm2," Opt. Lett. **32**(4), 358–360 (2007).
5. T. Hosaka, K. Okamoto, T. Miya, Y. Sasaki, and T. Edahiro, "Low-loss single polarisation fibres with asymmetrical strain birefringence," Electron. Lett. **17**(15), 530–531 (1981).
6. R. D. Birch, D. N. Payne, and M. P. Varnham, "Fabrication of polarisation-maintaining fibres using gas-phase etching," Electron. Lett. **18**(24), 1036–1038 (1982).
7. R. B. Dyott, J. R. Cozens, and D. G. Morris, "Preservation of polarisation in optical-fibre waveguides with elliptical cores," Electron. Lett. **15**(13), 380–382 (1979).
8. F. Couny, F. Benabid, P. J. Roberts, P. S. Light, and M. G. Raymer, "Generation and photonic guidance of multi-octave optical-frequency combs," Science **318**(5853), 1118–1121 (2007).
9. P. S. J. Russell, P. Hölzer, W. Chang, A. Abdolvand, and J. C. Travers, "Hollow-core photonic crystal fibres for gas-based nonlinear optics," Nat. Photonics **8**(4), 278–286 (2014).
10. F. Benabid and P. J. Roberts, "Linear and nonlinear optical properties of hollow core photonic crystal fiber," J. Mod. Opt. **58**(2), 87–124 (2011).
11. O. H. Heckl, C. R. E. Baer, C. Kränkel, S. V. Marchese, F. Schapper, M. Holler, T. Südmeyer, J. S. Robinson, J. W. G. Tisch, F. Couny, P. Light, F. Benabid, and U. Keller, "High harmonic generation in a gas-filled hollow-core photonic crystal fiber," Appl. Phys. B **97**(2), 369–373 (2009).
12. J. C. Knight, J. Broeng, T. A. Birks, and P. S. J. Russell, "Photonic band gap guidance in optical fibers," Science **282**(5393), 1476–1478 (1998).
13. P. J. Roberts, F. Couny, H. Sabert, B. J. Mangan, D. P. Williams, L. Farr, M. W. Mason, A. Tomlinson, T. A. Birks, J. C. Knight, and P. St. J. Russell, "Ultimate low loss of hollow-core photonic crystal fibres," Opt. Express **13**(1), 236–244 (2005).

#269041 http://dx.doi.org/10.1364/OE.24.022943
Journal © 2016 Received 23 Jun 2016; revised 15 Sep 2016; accepted 21 Sep 2016; published 26 Sep 2016

Optics EXPRESS

14. M. A. Duguay, Y. Kokubun, T. L. Koch, and L. Pfeiffer, "Antiresonant reflecting optical waveguides in SiO2-Si multilayer structures," Appl. Phys. Lett. **49**(1), 13 (1986).
15. N. M. Litchinitser, A. K. Abeeluck, C. Headley, and B. J. Eggleton, "Antiresonant reflecting photonic crystal optical waveguides," Opt. Lett. **27**(18), 1592–1594 (2002).
16. Y. Y. Wang, N. V. Wheeler, F. Couny, P. J. Roberts, and F. Benabid, "Low loss broadband transmission in hypocycloid-core Kagome hollow-core photonic crystal fiber," Opt. Lett. **36**(5), 669–671 (2011).
17. Y. Wang, F. Couny, P. J. Roberts, and F. Benabid, "Low loss broadband transmission in optimized core-shape kagome hollow-core PCF," in *Conference on Lasers and Electro-Optics 2010*, OSA Technical Digest (CD) (Optical Society of America, 2010), paper CPDB4.
18. F. Poletti, M. N. Petrovich, and D. J. Richardson, "Hollow-core photonic bandgap fibers: technology and applications," Nanophotonics **2**(5-6), 315 (2013).
19. F. Couny, F. Benabid, and P. S. Light, "Large-pitch kagome-structured hollow-core photonic crystal fiber," Opt. Lett. **31**(24), 3574–3576 (2006).
20. J. R. Hayes, F. Poletti, M. S. Abokhamis, N. V. Wheeler, N. K. Baddela, and D. J. Richardson, "Anti-resonant hexagram hollow core fibers," Opt. Express **23**(2), 1289–1299 (2015).
21. A. Hartung, J. Kobelke, A. Schwuchow, K. Wondraczek, J. Bierlich, J. Popp, T. Frosch, and M. A. Schmidt, "Double antiresonant hollow core fiber - guidance in the deep ultraviolet by modified tunneling leaky modes," Opt. Express **22**(16), 19131–19140 (2014).
22. A. D. Pryamikov, A. S. Biriukov, A. F. Kosolapov, V. G. Plotnichenko, S. L. Semjonov, and E. M. Dianov, "Demonstration of a waveguide regime for a silica hollow - core microstructured optical fiber with a negative curvature of the core boundary in the spectral region > 3.5 μm," Opt. Express **19**(2), 1441–1448 (2011).
23. A. N. Kolyadin, A. F. Kosolapov, A. D. Pryamikov, A. S. Biriukov, V. G. Plotnichenko, and E. M. Dianov, "Light transmission in negative curvature hollow core fiber in extremely high material loss region," Opt. Express **21**(8), 9514–9519 (2013).
24. W. Belardi and J. C. Knight, "Hollow antiresonant fibers with reduced attenuation," Opt. Lett. **39**(7), 1853–1856 (2014).
25. W. Belardi, "Design and properties of hollow antiresonant fibers for the visible and near infrared spectral range," J. Lightwave Technol. **33**(21), 4497–4503 (2015).
26. A. F. Kosolapov, G. K. Alagashev, A. N. Kolyadin, A. D. Pryamikov, A. S. Biryukov, I. A. Bufetov, and E. M. Dianov, "Hollow-core revolver fibre with a double-capillary reflective cladding," Quantum Electron. **46**(3), 267–270 (2016).
27. W. Belardi and J. C. Knight, "Hollow antiresonant fibers with low bending loss," Opt. Express **22**(8), 10091–10096 (2014).
28. B. Debord, M. Alharbi, L. Vincetti, A. Husakou, C. Fourcade-Dutin, C. Hoenninger, E. Mottay, F. Gérôme, and F. Benabid, "Multi-meter fiber-delivery and pulse self-compression of milli-Joule femtosecond laser and fiber-aided laser-micromachining," Opt. Express **22**(9), 10735–10746 (2014).
29. F. Emaury, C. J. Saraceno, B. Debord, D. Ghosh, A. Diebold, F. Gèrôme, T. Südmeyer, F. Benabid, and U. Keller, "Efficient spectral broadening in the 100-W average power regime using gas-filled kagome HC-PCF and pulse compression," Opt. Lett. **39**(24), 6843–6846 (2014).
30. F. Poletti, "Nested antiresonant nodeless hollow core fiber," Opt. Express **22**(20), 23807–23828 (2014).
31. J. M. Fini, J. W. Nicholson, B. Mangan, L. Meng, R. S. Windeler, E. M. Monberg, A. DeSantolo, F. V. DiMarcello, and K. Mukasa, "Polarization maintaining single-mode low-loss hollow-core fibres," Nat. Commun. **5**, 5085 (2014).
32. S. A. Mousavi, D. J. Richardson, S. R. Sandoghchi, and F. Poletti, "First design of high birefringence and polarising hollow core anti-resonant fibre," in *2015 European Conference on Optical Communication (ECOC)* (2015), pp. 1–3.
33. W. Ding and Y.-Y. Wang, "Hybrid transmission bands and large birefringence in hollow-core anti-resonant fibers," Opt. Express **23**(16), 21165–21174 (2015).
34. P. J. Roberts, "Birefringent hollow core fibers," Proc. SPIE **6782**, 67821R (2007).
35. F. Poletti, N. G. R. Broderick, D. Richardson, and T. Monro, "The effect of core asymmetries on the polarization properties of hollow core photonic bandgap fibers," Opt. Express **13**(22), 9115–9124 (2005).
36. X.-L. Tang, B.-S. Sun, and Y.-W. Shi, "Design and optimization of low-loss high-birefringence hollow fiber at terahertz frequency," Opt. Express **19**(25), 24967–24979 (2011).
37. P. J. Roberts, D. P. Williams, H. Sabert, B. J. Mangan, D. M. Bird, T. A. Birks, J. C. Knight, and P. S. J. Russell, "Design of low-loss and highly birefringent hollow-core photonic crystal fiber," Opt. Express **14**(16), 7329–7341 (2006).
38. J. Hayes, S. Sandoghchi, T. Bradley, Z. Liu, R. Slavík, M. A. Gouveia, N. Wheeler, G. Jasion, Y. Chen, E. Numkam-Fokoua, M. Petrovich, D. Richardson, and F. Poletti, "Antiresonant hollow core fiber with octave spanning bandwidth for short haul data communications," in *Optical Fiber Communication Conference Postdeadline Papers* (Optical Society of America, 2016), p. Th5A.3.
39. C. Wei, R. A. Kuis, F. Chenard, C. R. Menyuk, and J. Hu, "Higher-order mode suppression in chalcogenide negative curvature fibers," Opt. Express **23**(12), 15824–15832 (2015).
40. M. Michieletto, J. K. Lyngsø, C. Jakobsen, J. Lægsgaard, O. Bang, and T. T. Alkeskjold, "Hollow-core fibers for high power pulse delivery," Opt. Express **24**(7), 7103–7119 (2016).
41. L. Vincetti and V. Setti, "Waveguiding mechanism in tube lattice fibers," Opt. Express **18**(22), 23133–23146 (2010).
42. E. A. J. Marcatili and R. A. Schmeltzer, "Hollow metallic and dielectric waveguides for long distance optical transmission and lasers," Bell Syst. Tech. J. **43**(4), 1783–1809 (1964).

Optics EXPRESS

1. Introduction

Besides loss, bandwidth and modal properties, the ability to control and maintain the polarization state (e.g. by inducing a large birefringence or a differential loss between the two orthogonally polarized modes) is a key feature for a wide range of optical fiber applications, including precise interferometric sensing (e.g. fiber based gyroscopes [1]), quantum computing [2], atom spectroscopy [3], and polarization maintaining optical amplifiers [4]. Although conventional polarization-maintaining (PM) fibers have been around for many years, in which a high birefringence (Hi-Bi) is introduced by applying either stress (e.g. PANDA or Bow-tie fibers [5, 6]) or form anisotropy (e.g. elliptic core [7]), they face a few fundamental limitations associated with their solid core. For example, material absorption, low damage thresholds and optical nonlinearity fundamentally restrict their application to wavebands where the glass is transparent and to optical powers low enough not to cause undesired nonlinear effects and/or dielectric damage. Some of these limitations can be addressed by using hollow core optical fibers, which in addition can also enable interesting new linear and nonlinear applications exploiting long path lengths for gas-light interactions [8–11]. Despite many potential advantages, hollow core fibers are a less mature technology than solid core versions, which still require physical understanding and new optical designs in order to achieve their full potential. In general, there are two major hollow core fiber categories in terms of transverse modal confinement mechanism: photonic bandgap fibers (HC-PBGFs), which rely on the creation of a photonic band gap in the cladding [12, 13] and anti-resonance fibers (HC-ARFs) where guidance occurs as a result of antiresonant effects in glass membranes surrounding the fiber core [14, 15], and is strengthened by inhibited coupling between core (air) and cladding (glass) modes [16, 17].

So far, HC-PBGFs have demonstrated lower loss than HC-ARFs [13, 18]. However, their narrow bandwidth (i.e. 10-30% of the central operating wavelength) and larger field overlap with the glass in comparison to HC-ARFs [9] make them less suitable for broadband applications (e.g. broadband nonlinear processes) or for high power delivery. During the last decade considerable research has focused on lowering the loss in HC-ARFs and many different structures have been proposed based on: a Kagomé cladding [16, 19], a hexagram structure [20], a double anti-resonance layer [21], tubular “negative curvature” structure [22, 23] and nested tubular structure [24–26]. These have resulted in significant improvement of properties such as low bend-loss [27], ultra-large bandwidth [8] and high damage-threshold [28, 29]. In addition to the above, the recent nested antiresonant nodeless hollow core fiber (NANF) design, which incorporates nested glass rings, has the potential to achieve loss levels as low as that of solid core fibers [30].

Generating a birefringence of the same order of magnitude as in commercial solid core PM fibers (~10^{-4} for 1550nm operation) in a hollow core fiber is however difficult. Conventional methods of using stress rods (and, as we shall see, elliptical shapes) are not applicable or effective. Besides, structural requirements to minimize confinement loss in hollow core fibers add additional limitations. Arguably, the best result so far was achieved in a HC-PBGF with asymmetric rods in the core surround, presenting low loss (10dB/km at 1.530μm) and birefringence in the range of that of solid-core fibers, albeit over a narrow operating bandwidth (<10nm) [31]. Achieving such a high birefringence in HC-ARFs is even harder since the field overlaps with glass and the resulting sensitivity of the birefringence to the core’s geometry is even lower. Only recently, two theoretical Hi-Bi HC-ARFs based on modified NANF concepts were proposed which could address the problem by operating in the normal [32] or hybrid band transmission regimes [33]. Both show promising routes to achieve high birefringence (~10^{-4}) in ARFs. However, the underpinning differences between the two approaches require detailed study, and further reduction of the loss and widening the Hi-Bi bandwidth are still possible and as targeted here.

In this paper, we report a detailed study of the birefringence of NANF designs that have tubes with different membrane thicknesses along orthogonal axes (bi-thickness NANFs) and propose a design procedure to maximize the bandwidth and minimize loss while maintaining

Optics EXPRESS

high birefringence operation. In the following Section, we demonstrate that unlike solid fibers, an elliptical core shape cannot provide a large enough birefringence in a hollow core fiber. In Section 3, we propose a way to circumvent this using a bi-thickness NANF with a small core and 4 triple nested tubes. We also introduce an approach for analyzing the effect of the design parameters of the fiber on its loss, bandwidth and regime of operation, using this we propose a new HC-ARF design providing the lowest loss and the widest bandwidth high birefringence operation ever reported, to the best of our knowledge. In Section 4, we propose for the first time, the out-stripping of one selected fundamental polarization mode to provide the hollow core fiber with an additional polarizing ability, in addition to a polarization maintaining behavior. We finally summarize our work in Section 5.

2. Birefringence by asymmetry

While the PM property of HC-PBGFs has already been investigated theoretically in various works [34, 35] and promising results have been achieved experimentally [31], extending these results to anti-resonance fiber types is not straightforward, and only recently the first designs have been proposed [32, 33]. In general, symmetrically arranged HC-ARFs can support degenerate polarization modes and polarization coupling due to random perturbations is inevitable. The idea of breaking the core symmetry and introducing ellipticity in the antiresonant reflecting optical waveguide (ARROW)-guiding fibers has therefore been investigated in some of the simplest structures for terahertz applications [36], following the idea of exploiting form-birefringence that is used in solid core PM fibers. In this work, to study the potential of generating polarization mode birefringence (PMB) through core ellipticity in HC-ARFs, we start by considering an ideal elliptical tube as the simplest possible HC-ARF structure. The thickness of the tube needs to satisfy the resonance equation of ARROWs in order to support the leaky fundamental mode (FM) at frequencies f in the desired (m^{th}) anti-resonance band [30]:

$$\frac{c.(m-1)}{2t_1\sqrt{n_2^2-n_1^2}} < f < \frac{c.m}{2t_1\sqrt{n_2^2-n_1^2}}, \qquad m = 1, 2, \ldots . \tag{1}$$

where c is the speed of light in vacuum. n_1, n_2 and t_1 are the refractive indices of core, clad and the thickness of the tubes, respectively. Using Eq. (1) and choosing an operating wavelength (λ_0 = 1.55μm) in the second anti-resonance band, a thickness t_1 = 1.172μm is estimated to produce the lowest loss for a core radius of R = 10μm. In order to investigate the effect of the tube's ellipticity on its PMB, elliptical tubes with different major (b) to minor (a) axis ratios have been simulated by using a commercial finite element (FEM) mode solver (Comsol®) with optimized meshes and perfectly matched absorbing boundary layers [30]. Figure 1 shows the simulated confinement loss and PMB ($N_{V/H}$ = effective index of vertical/horizontal polarization) of the FM for different tube core dimensions. The simulation result shows that the PMB initially increases on increasing the ellipticity of the core, as shown in Fig. 1(a). However, after a peak around b/a ~1.6, it decreases and settles to an almost constant value for further increase in the ellipticity, regardless of the core size. This indicates an optimum point for ellipticity. Additionally, it is seen that decreasing the core size to achieve a discernible PMB is necessary. However, as shown in Fig. 1(c), reducing the core size results in impractically large loss, which in practice limits the minimum core size one can choose.

It is well known that loss in an antiresonant HC fiber can be reduced by designing the core surrounding membranes with negative curvature [16, 17, 22]. Amongst various designs, the NANF structure has shown the potential for very low optical loss, in principle comparable to that of solid silica fibers [30]. This structure consists of a number of equally spaced non-touching nested glass tubes, as shown in Fig. 2(a), which are attached to the inner wall of a larger jacket tube. The nested tube arrangement provides the anti-resonant cladding of the fiber, with the hole in the middle acting as the core. In this design, confinement loss is reduced dramatically due to the absence of nodes in the core surround, which can induce

Optics EXPRESS

undesired coupling to lossy cladding elements (e.g. membranes) [20], and to the addition of coherent radially arranged reflecting layers. One might therefore want to consider whether a NANF with an elliptical cross section (and a small core) might provide a way to generate a significant PMB and low loss. The simulated loss and PMB of an elliptical core NANF obtained by rearranging and reducing the size of two opposite sets of nested tubes (see bottom structure in Fig. 1(b)) for different ellipticity is shown with markers in Fig. 1, and compared with the behavior of an elliptical tube. For both structures, a reduction in core size is helpful in increasing the birefringence, but at all core sizes the birefringence peaks around an optimum value of ellipticity for each core size. Larger ellipticities than that do not produce any higher birefringence.

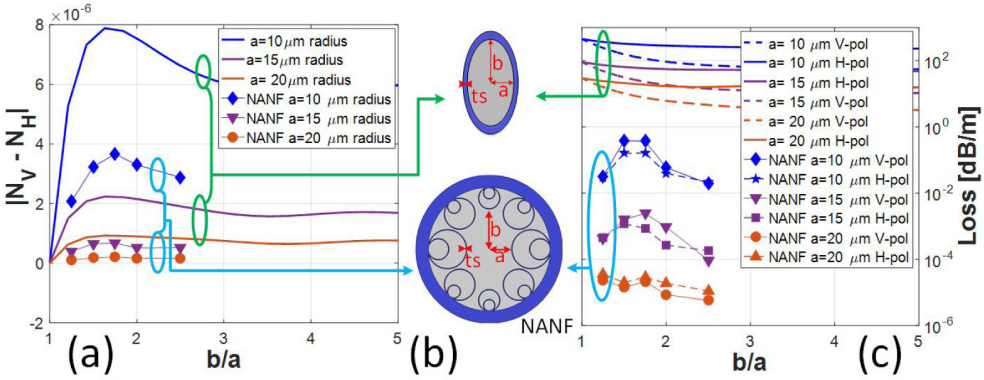

Fig. 1. The characteristic profile of a single tube for different minor axis (a = 10μm, 15μm, 20μm) vs major axis b with t_s = 1.172μm at λ_0 = 1.55μm. (a) Birefringence of the fibers for different ellipticity, (b) tube structure (top) and NANF structure (bottom), (c) loss profile of fibers for horizontal and vertical polarization for different ellipticity. Properties of elliptical core NANF for a = 10μm, 15μm at optimum ellipticity are provided for comparison.

As the results suggest, although the NANF structure can reduce the loss by many orders of magnitude in comparison to single tube, the resultant PMB of only 1-2 × 10^{-6} is too low for PM operation. Additionally, to increase the PMB in NANF fibers by form-birefringence, we have explored other geometrical arrangements of the nested tubes that provide a large core ellipticity, as shown in Fig. 2(b). However, our simulations show that despite the fairly large core ellipticity achieved in these fibers (b/a> 2), the PMB remains below ~10^{-5} in all cases.

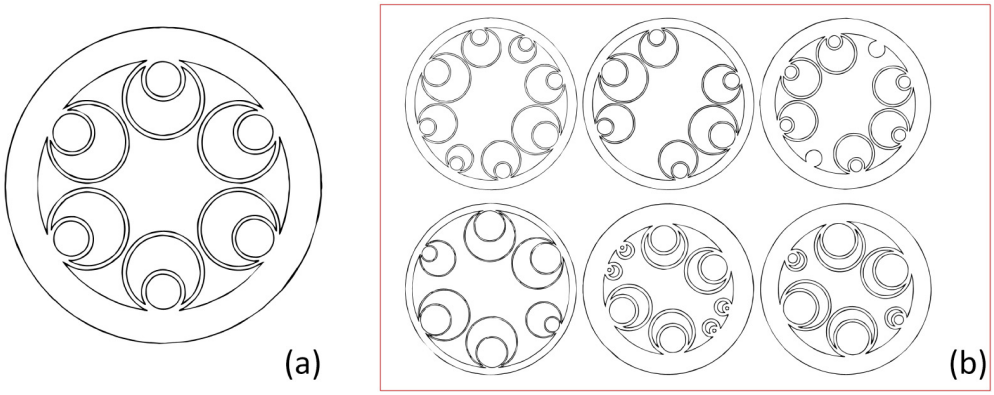

Fig. 2. (a) 6 tube NANF design, (b) alternative NANF with elliptical core designs studied in this work, which we found to be unable to provide birefringence >10^{-5}.

In conclusion, the achievable PMB by making the air hole elliptical is not adequate to guarantee the HC-ARF a PM behavior in the visible/infrared regions of the electromagnetic

Optics EXPRESS

spectrum. However, there are some examples of multilayer ARROW fibers with large enough PMB factor at longer operating wavelengths (THz guidance) [36].

3. Birefringence in bi-thickness NANFs

In addition to elliptical core designs, another potential approach to induce significant birefringence in ARFs has been proposed and has previously been commercially exploited in HC-PBGFs [31] This relies on introducing a controlled anti-crossing between air-guided and glass-guided (surface) modes. By using glass elements of different thickness along orthogonal directions in the core surround, a significantly different effective index for the two polarizations of the FM can be achieved at the edge of an anti-crossing point [37]. In this way the birefringence is introduced by anti-crossing phenomena rather than by geometrical asymmetry [34].

Whilst this has only been experimentally applied to PBGFs so far, a couple of theoretical studies have explored the extent to which the concept can be applied to ARFs that guide light through a different physical mechanism [32, 33]. The main idea is to generate birefringence by introducing an asymmetry through modifying the thickness of selected core surrounding membranes in ARFs. Horizontal and vertical glass membranes can operate in either the same antiresonant window [32] or in a so called "Hybrid" regime where they operate in different anti-resonance bands with opposite locked field phases at the outer boundaries [33]. In this work, we undertake a systematic study of both operating regimes, highlighting their benefits and drawbacks. Additionally, we show that by applying a suitable modification to the design of a state-of-the-art NANF, not only it is possible to enhance its birefringence and therefore its polarization maintaining behavior, but also to achieve a broad bandwidth that spans several 100s nm at a low enough loss for most device and power delivery applications.

3.1 The effect of thickness change on birefringent NANF

Following the abovementioned strategy (de-symmetrizing by an appropriate modification of the thickness of some glass membranes), one could think of a 6-tube low-loss NANF [30] and change the thickness of two oppositely located nested tubes with a different thickness than the remaining four. By simulating ANFs with 3 to 8-tubes of two different thicknesses, however, we have found that a structure with 4-tubes can achieve a considerably higher birefringence, as shown in Fig. 3. We believe that the orthogonality of the core surrounding glass webs to the polarization of the core field is key to explain these effects. The fiber with 4 tubes is the only geometry able to guarantee membranes that are orthogonal to the mode polarization This effect can also be explained by the tendency of each polarization of the FM at the edge of the anti-crossing frequency to couple preferentially to cladding tube modes with a similar polarization [33, 35].

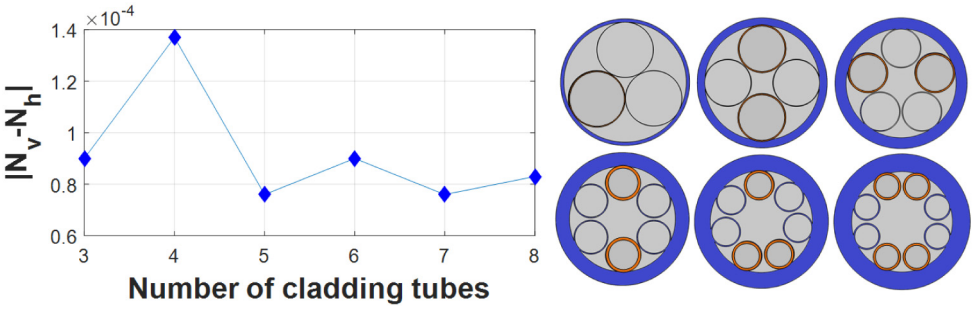

Fig. 3. Birefringence (N_v-N_h) of 3-tube to 8-tube ANF design at λ_0 = 1.55µm alongside their structures with same core size (R = 7µm) and bi-thickness cladding tubes (thin tubes (blue) = 0.372µm and thick tubes (orange) = 0.633µm). The 4-tube structure shows maximum birefringence, and the structures with odd number of tubes show lower birefringence due to lack of 2-fold symmetry.

Optics EXPRESS

It is also noticeable that structures with odd number of tubes show lower birefringence, which can be explained by their lack of 2-fold symmetry, resulting in worse orthogonality between core boundaries and direction of polarization of the fundamental modes. We leave this topic open for further investigation in future works.

Since the 4-tube fiber was found to offer higher birefringence, the rest of the paper will focus on this structure and further optimize its performance.

Our starting point is a 4-tube NANF in which the tubes aligned along the vertical axis have a thickness t_1 which can be the same (normal operation) or different from that (t_2) of the tubes along the horizontal axis (i.e. a bi-thickness fiber). In order to minimize the loss while maintaining a small enough core to provide large birefringence in air (see section 2), we chose a design with two nested tubes inside a larger external one, as shown in Fig. 4(a), which details all the relative design parameters. In order to optimize the confinement loss for a core radius of R = 7μm and an azimuthal tube distance d = 1.5 μm, the distance between the inner tubes (z) was calculated using the quarter wave condition which ensures the in-phase reflection of each layer towards the core [20]:

$$z \approx \frac{\pi}{2u_0} R \approx 0.65R. \tag{2}$$

where u_0 is the solution of the first zero of the zeroth order Bessel function. Depending on the choice of t_1 and t_2, the fiber can operate in the following three regimes:

1. Non-birefringent guiding (standard operation, see Fig. 4(b)): $t_1 = t_2$ and the fiber shows no birefringence.
2. Same band birefringent operation: t_1 and t_2 are slightly different so that anti-crossing shifted birefringence is obtained whilst anti-resonance occurs in the same window for both FM polarizations.
3. Different band birefringent operation: t_1 and t_2 are considerably different, such that the anti-resonance in the orthogonal directions occurs in different bands and the FM polarizations have opposing locked field-phase at the outer boundaries (hybrid regime birefringence) [33].

As a starting point we begin with a uniform NANF ($t_1 = t_2$). Using Eq. (1), a thickness $t_1 = t_2 = 0.6$μm is selected such that the fiber operates in the first anti-resonance band around near-IR telecoms wavelengths (~1.55μm). Figure 4(b) shows the effective refractive index (N_{eff}) and loss profile of the designed fiber. The target operating wavelength of 1.55μm has been placed within the first anti-resonance band but not at the lowest loss point, for the purpose of examining different scenarios. The fiber, as expected, shows no birefringence. However, the fiber's polarization properties change dramatically when the thickness of all tubes along one axis is modified. Figure 5 shows the evolution of the loss for each FM polarization and the effective index difference at $\lambda_0 = 1.55$μm when t_2 is changed for a fixed $t_1 = 0.6$μm. It worth mentioning that increasing t_2 causes the inner radii of the corresponding tubes to decrease, while the other parameters remain unchanged.

At $t_2/t_1 = 1$ the fiber presents no birefringence and operates in the first anti-resonance band. As the thickness of the horizontal tubes (t_2) increases, the resonance region of these tubes start to shift towards the wavelength $\lambda_0 = 1.55$μm while the vertical tubes do not shift and still work around the original anti-resonance condition. The induced birefringence under this condition can be explained in various ways through:

a) the different behavior between parallel and perpendicular polarization of core modes at the anti-crossing point [34];

b) the close relationship between the increase in N_{eff} and the sharp rise in confinement loss based on the Kramers-Kronig relation, which is caused by the reduction in anti-resonance reflection of the glass membranes at the edge of the resonance frequency band [33];

Optics EXPRESS

c) the difference in confinement radius (not to be confused with the geometrical radius) of the individual fundamental polarization modes for different thicknesses, which cause a change in N_{eff} that can be explained by the well-known connection between mode radius and N_{eff} in an anti-resonance structure [33].

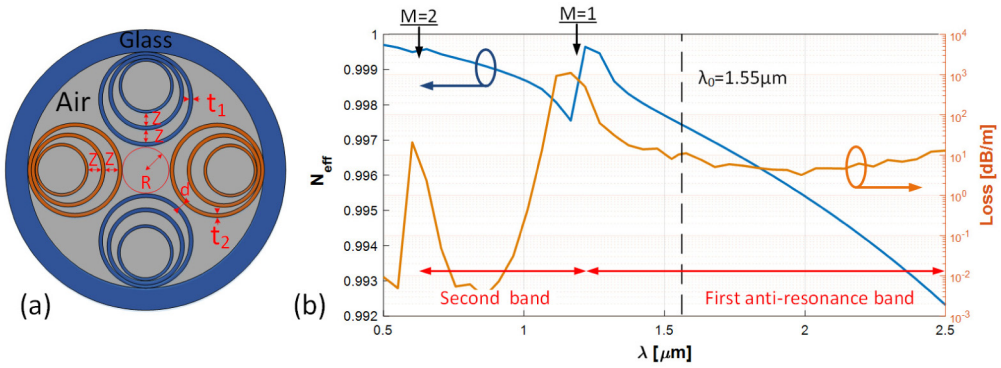

Fig. 4. (a) Bi-thickness NANF and its design parameters, (b) simulated optical performance of a uniform NANF with t1 = t2 = 0.6μm, R = 7μm, d = 1.5μm and z = 0.65R.

As t_2 continues to increase, its associated resonance frequency reaches λ_0, which induces a large loss, marked as "resonance region" in Fig. 5. Beyond this point, the birefringence repeats the previous pattern, with fairly large (>10^{-4}) positive and negative values achievable. However, in this case the horizontal tubes operate in a higher anti-resonance band (second band when t_2/t_1 = 1.5-2.3, or third band when t_2/t_1 = 2.7-3.6). Moreover, a zero birefringence crossing is obtained for certain thicknesses. Interestingly, as Fig. 5(a) shows, while the vertical polarization (V-pol) experiences a similar loss as for t_2/t_1~1, the loss of the horizontal polarization (H-pol) decreases by as much as two orders of magnitude; a feature that can be exploited in a polarizing fiber design.

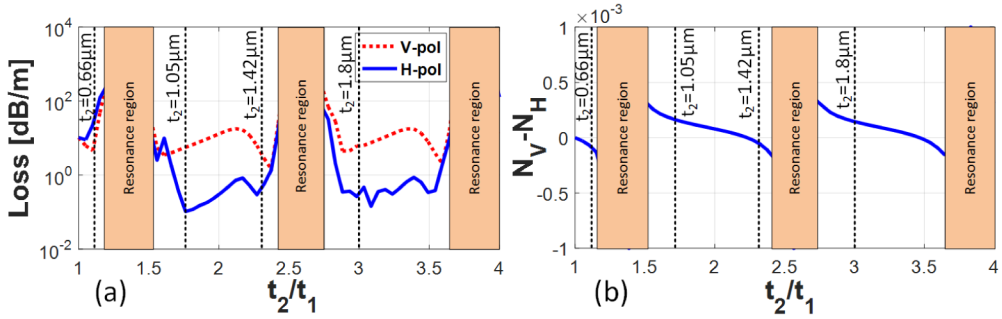

Fig. 5. Optical properties of the NANF in Fig. 4(a) (t_1 = 0.6μm, R = 7μm, d = 1.5μm, z = 0.65R) at λ_0 = 1.55μm as t_2 / t_1 varies between 1 and 4: (a) polarization mode loss, (b) birefringence.

As shown above, sweeping t_2 provides a good design tool to find the highest possible birefringence at a single wavelength for a pre-determined t_1. However, the effect of the initial choice of t_1 on loss, and the mutual effect of t_1 and t_2 on the bandwidth over which a large birefringence is achieved are not fully explained by the above picture. In the next section, we study the characteristic profile of different combinations of fibers in order to draw a clearer picture of the role of each design parameter.

3.2 Bi-thickness NANF: a systematic study

In order to study the behavior of the fiber for different combinations of thicknesses (t_1, t_2) and working regimes, we simulated the spectral characteristics (i.e. loss and birefringence vs

Optics EXPRESS

wavelength) for several combinations of thicknesses (t_1, t_2) from Fig. 5 as highlighted by the dashed lines. Each combination case represents a different working regime in order to highlight the mutual effect of t_1 and t_2 on loss, birefringence and bandwidth. Figure 6 shows the results for fibers with t_1 = 0.6μm, and t_2 = 0.66, 1.05, 1.42 and 1.8 μm, alongside the non-birefringent NANF case (Fig. 6 (a)). We defined a practical working condition for the fibers, where the combination of birefringence and loss is reasonable. That is a loss lower than 1dB/m (practical loss for most short length applications) and a birefringence with a beat length smaller than 15.5 mm (corresponding to a birefringence of 10^{-4} at 1.55μm - the same order of magnitude as conventional solid-core PM fibers). These regions correspond to below the red dashed-line in the loss curve and outside the red dashed-line box in the birefringence plots.

Starting with the case t_2 = 0.66μm, the loss shows only a slight difference for the perpendicular FM polarization and some birefringence starts to appear, although this is still rather modest in magnitude, as shown in Fig. 6(b). The fiber therefore does not meet the defined loss and birefringence criteria.

Beyond a certain thicknesses, the resonance region of the horizontal tubes falls after λ_0. For t_2 = 1.05μm, a large birefringence and acceptable loss can be observed as shown in Fig. 5. Figure 6(c) shows the optical properties of the fiber in this case. Here, the second resonance wavelength of t_2 has become large enough to reach the first resonance wavelength of the thinner tubes (t_1) (m_{t2} = 2 in Fig. 6(c)). The fiber has an acceptable low loss window in the Hi-Bi region between the two resonances m_{t2} = 1 and 2. In fact, as shown earlier, only one polarization of the fiber has a lower loss as compared to the symmetric fiber. This behavior can be explained by the fact that the loss associated with each polarization of a FM is mainly controlled by the membranes perpendicular to the electric field of the mode, and operation in the second window creates a lower leakage loss than in the first one. That is, in this case, the losses of the horizontal/vertical polarization mode, which are perpendicular to the thicker/thinner tubes (t_2/t_1), are determined mainly by the anti-resonance condition of the perpendicular tube, respectively.

As a result, compared to the uniform NANF, the H-pol experiences a lower loss as the thicker tubes (t_2) are working in the second anti-resonance band, while the loss of the V-pol is dominated by the thinner tubes (t_1), which operate in the first anti-resonance band and shows higher loss. In other words, the bi-thickness fiber operates on each individual polarization in the same way as a uniform fiber with tubes as thick as the tubes perpendicular to the electric field of that polarization.

Since the overlap between second and first anti-resonance bands of t_2 and t_1 respectively provides a good window of operation, we studied the possibility to shift the first resonance of t_2 further towards longer wavelengths in order to widen its second anti-resonance band. To examine this approach, we simulated a bi-thickness fiber with t_2 = 1.42μm (see Fig. 5), with the results shown in Fig. 6(d). At a first glance, the bandwidth of low loss operation has increased. However, the birefringence of the fiber has significantly reduced. A closer look reveals a zero birefringence crossing in this region. This is a characteristic feature of this region, which essentially limits the bandwidth of high birefringence achievable. It is caused by the fact that the second window is narrower than the first and hence has a steeper dispersion, which inevitably crosses that of the first window.

To include other possibilities and to study a broader span of thicknesses, we have finally considered t_2 = 1.8um, chosen from the third region of Fig. 5 with high birefringence and low loss. In this case, as it can be seen in Fig. 6(e), three anti-resonance bands of t_2 overlap with the first anti-resonance band of t_1. While the first one (at λ>3um, not shown) has a very high loss, the second and third bands show low loss operation. In this case, similar to the previous case (t_2 = 1.42μm), a zero-crossing occurs in the second band which limits its bandwidth significantly. However, there is a small high birefringence window overlapping with a low loss band, which provides a good operational window in the third anti-resonance band, as shown by the green arrows in Fig. 6(e). Here, some features are noticeable in the characteristic profile of this fiber. For instance, the third anti-resonance band shows almost

Optics EXPRESS

identical birefringence and loss profiles to the second band in the case with t_2 = 1.05μm, which demonstrates that it is possible to achieve Hi-Bi even in the same outer locked field phase condition (third band over first band), see [29]. In other words, the existence of the "Hybrid" regime [33] is not necessary to achieve Hi-Bi and low loss simultaneously. However, as the bandwidth of the third anti-resonance band is intrinsically smaller than the second one, the achievable birefringence bandwidth in this region is generally narrower.

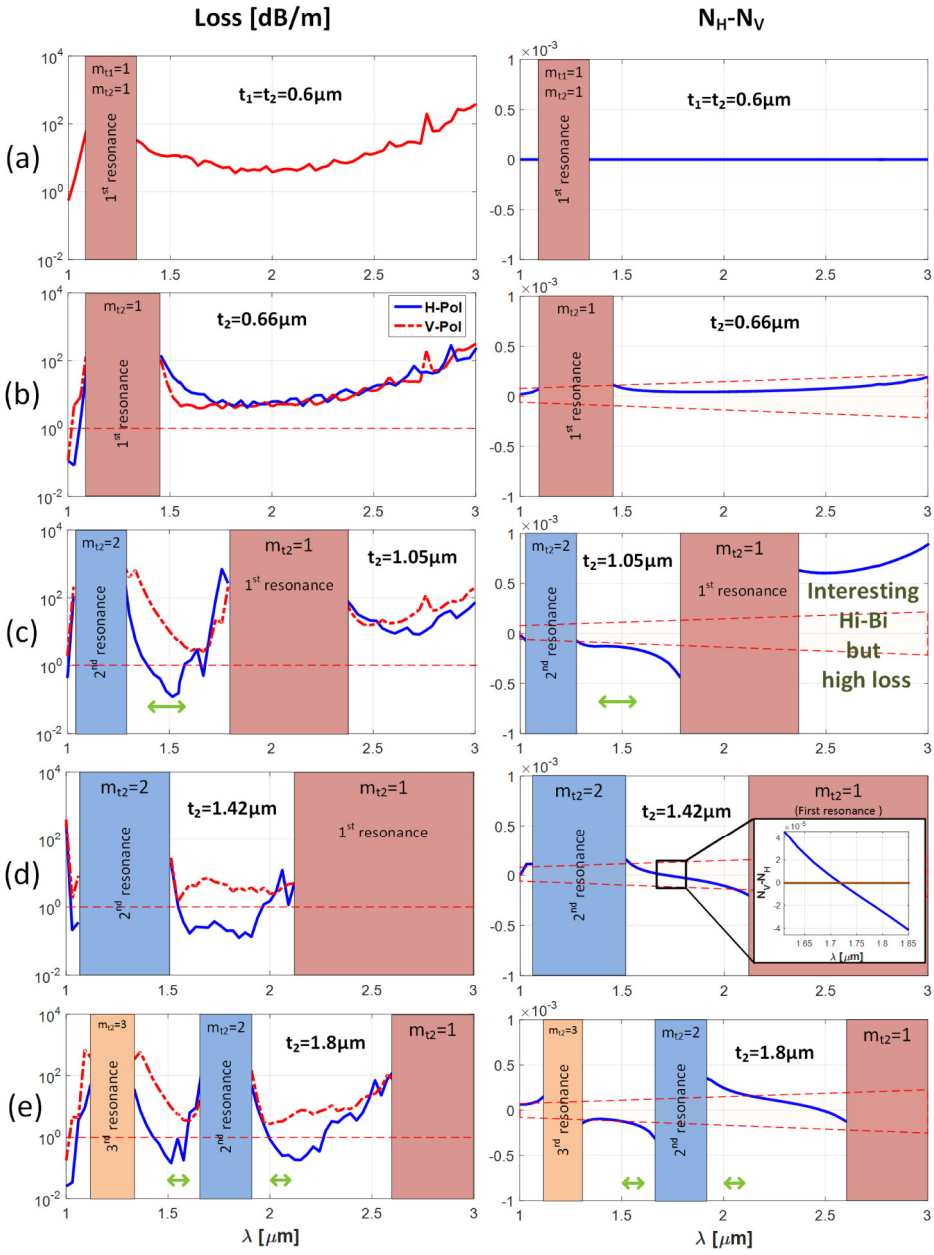

Fig. 6. Simulated loss and birefringence profile of a bi-thickness 4 tube NANF with t_1 = 0.6μm, R = 7μm, d = 1.5μm and t_2 = 0.6, 0.66, 1.05, 1.42 and 1.8μm ((a) to (e) respectively). The red dashed line in the loss profile shows 1 dB/m and the red dashed lines in the birefringence profile indicates a beat length equal to 15.5 mm (roughly the birefringence of a conventional solid-core PM fiber). The green arrows show the defined practical operating window with loss lower than 1 dB/m and beat length larger than 15.5 mm.

Optics EXPRESS

Amongst all explored scenarios, just three practical regions can be used to simultaneously achieve Hi-Bi and low loss, as shown by green arrows in Fig. 6. A) The region right after, where the second resonance of t_2 and the first resonance of t_1 overlap (case t_2 = 1.05μm); B & C) The regions where the third and second anti-resonance band of t_2 and the first anti-resonance band of t_1 overlap (case t_2 = 1.8μm). Although the regions of interest show high birefringence and low loss, their bandwidth is limited not only by the intrinsic bandwidth of their anti-resonance band, but also by the abrupt loss increases near the resonance regions. Additionally, we have shown that shifting the second resonance away from the first one has some limitations due to the presence of a birefringence zero-crossing, which prevents ultra-broad band operation (Fig. 6 (d)).

Figure 6 also shows another region of potential interest, the broad Hi-Bi region in the first anti-resonance band of the fiber with t_2 = 1.05μm (Fig. 6(c)). This spectral range has intrinsically the largest possible bandwidth between all the cases as it is placed in the first anti-resonance band of both t_1 and t_2, simultaneously. However, despite its Hi-Bi and broadband feature, this region suffers from a high loss because it is close to the edge of the resonance of t_2 and operates in two different parts of the same anti-resonance band of t_1 and t_2. The next section focuses on improving the loss of this region.

3.3 Modified bi-thickness NANFs

In order to achieve broadband and large birefringence that benefits from the potential of the first anti-resonance band, we need to overcome its large loss through a modified design. Here, we propose a structure that has reduced loss at the edge of an anti-crossing by eliminating the in-phase resonance layers. The proposed structure exploits anti-resonant inner tubes operating at the optimum point to minimize the loss in the first anti-resonance band, while the birefringence is still induced by the change in the thickness of the outer tubes. Figure 7(a) shows the proposed modified structure and its design parameters. Figures 7(b) and (c) show the performance of the proposed fiber with similar parameters as those presented in Fig. 6(c), alongside the properties of a normal bi-thickness fiber with similar parameters, shown in Fig. 7(d) (a duplicate of Fig. 5(c) for ease of comparison).

A significant loss reduction is achieved in the first anti-resonance band of our new design, reducing the minimum loss below 1dB/m, while the loss increases in the second anti-resonance band compared to the previous fiber, as shown in Fig. 7(c). Differently from the bi-thickness structure of Fig. 4 (a), in this arrangement, similar thickness t_1 of all the inner tubes guaranties an improved in-phase field confinement with lower loss in the first anti-resonance band, whilst a large birefringence through the outer tubes (t_2) is achievable. In the proposed structure, the dominant contribution to confinement is provided by t_1 for both polarizations, while in the original bi-thickness structure, t_1 and t_2 almost independently control the loss of the perpendicular polarization modes. This feature in the new design not only gives the ability to minimize the loss by optimizing only one thickness, but also increases the possible tuning range of t_2 to provide larger and broader birefringence outside its resonance by eliminating the strong dependency of loss on this parameter.

Although the design in Fig. 7 shows improvements in terms of loss and birefringence in the first antiresonant window, its parameters are not optimized for the lowest loss and largest operating bandwidth. To obtain the optimum design at the operating wavelength λ_0 = 1.55μm, we started by considering a uniform NANF with single thickness t_1. We used Eq. (1) to calculate a starting value for t_1. Then, we refined the thickness t_1 using a parametric sweep simulation to achieve the lowest loss at the first anti-resonance band, which resulted in t_1 = 0.372μm. Then we introduced the thicker tubes with thickness t_2 in the design. Using another parametric sweep similar to Fig. 5, t_2 was optimized to provide the highest birefringence. The result is a bi-thickness 4-tube NANF with t_1 = 0.372μm, $t_2 = 1.7t_1$, R = 7μm, d = 1.5 μm and z = 0.65R. Figure 8 shows the simulated properties of the optimized Hi-Bi NANF with improved loss in the first anti-resonance band around λ_0 = 1.55μm.

Optics EXPRESS

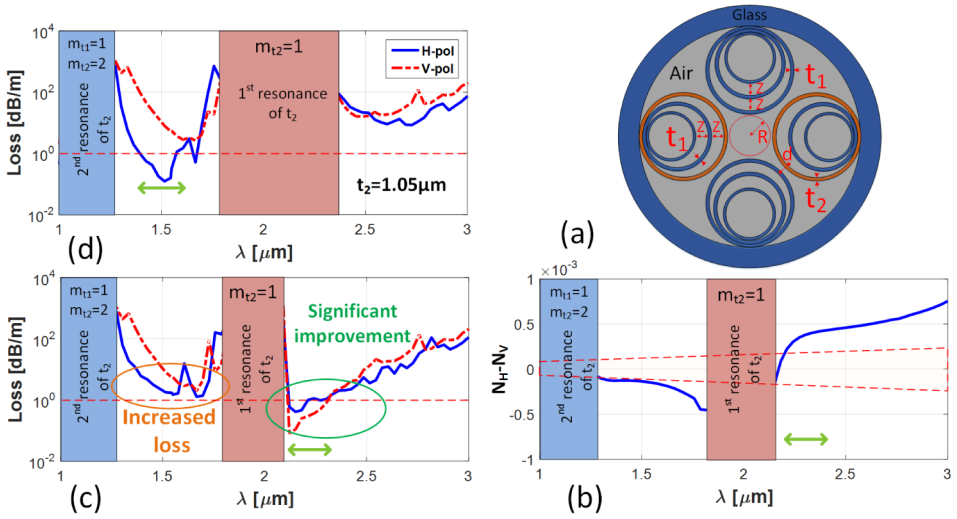

Fig. 7. Proposed modified bi-thickness NANF: (a) structure; (b) birefringence and (c) loss of the proposed NANF with the same parameters as in Fig. 6(c), (d) loss of standard bi-thickness NANF (duplication of Fig. 6(c) for comparison). Anti-resonant field confinement by inner tubes of thickness t_1 provides a significant improvement in the loss of the first anti-resonance region.

This design and method, not only reduces the loss for both polarizations over several hundred of nm, but also increases the birefringence of the fiber simultaneously. Using this design strategy, we achieved an anti-resonance hollow core fiber with ultra-broadband high PMB and sub dB/m loss. The fiber has a birefringence of ~1.5 × 10^{-4} over a ~550nm bandwidth (loss <1dB/m) with a minimum loss as low as 0.043dB/m at λ_0. The proposed fiber is therefore ideally suited for ultra-broadband applications requiring polarization maintenance over almost all optical communication bands (E, S, C, L and U bands).

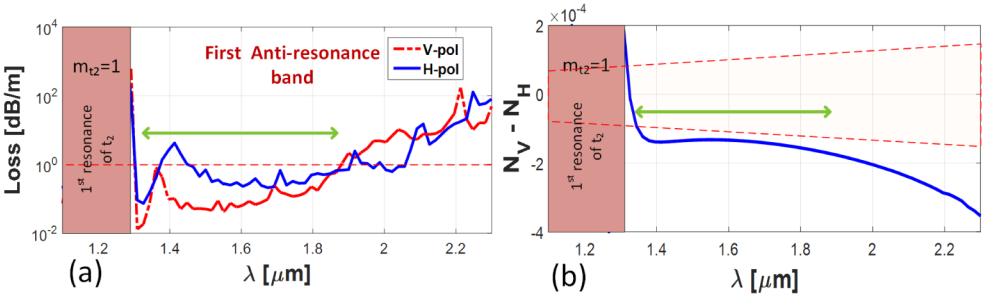

Fig. 8. (a) Loss and (b) birefringence of the optimized new proposed design for λ_0 = 1.55µm with R = 7µm, Z = 0.65R, d = 1.5µm, t_1 = 0.372µm and t_2 = 0.633µm. The fiber shows a very broad bandwidth (~550nm) PMB = ~1.5 × 10^{-4} with a loss <1dB/m.

Figure 9 shows the mode profile of both FM polarizations at λ_0. As can be seen, the outer horizontal thicker tubes (t_2) provide lower reflectivity for the horizontal mode, as they operate at the edge of the resonance window, allowing some of the field to leak. However, the inner rings, which operate in perfect anti-resonance conditions, reduce the leakage of the field. As a result, the loss of the horizontal mode is only slightly higher than that of the vertical one whereas a large birefringence is obtained.

In practice, the proposed tube thicknesses in our design are achievable and have already been demonstrated in simpler single ring tubular fibers [38]. However, in order to relax the requirement for thin tubes and to allow easier fabrication, one can design the fiber to operate in the second anti-resonance window, if the full 550nm of low loss PM operation are not

Optics EXPRESS

strictly required. Figure 10 shows the optical properties of such an alternative fiber with thicker tubes operating in the second anti-resonance band (t_1 = 1.172 µm, t_2 = 1.42µm).

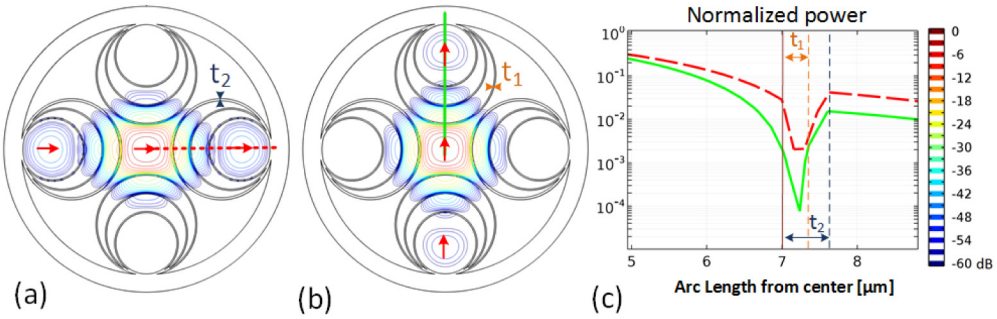

Fig. 9. 3-dB contour plots of the normalized power of the fundamental mode with (a) horizontal and (b) vertical polarizations (red arrows indicate the direction of the electric field) at λ_0 = 1.55µm for the optimum proposed design. (c) Cross-sectional profile of the normalized power in each polarization direction. A larger field penetration through the outer horizontal tubes (t_2) than the vertical ones (t_1) is clear while the horizontal inner tubes (t_1) play a critical rule in confining the field and reducing the loss.

This fiber shows an almost constant PMB value as large as ~1.45×10^{-4} with loss <1dB/m over a ~300nm bandwidth covering the entire C, L and U optical communication bands. The loss in this design reaches its lowest value of 0.006dB/m at λ = 1.57µm, and is around 0.01dB/m across the C + L bands. In comparison, based on our simulations, a fiber with a similar core size in the hybrid regime (see Section 3.2 and [33]) has a loss value that is more than 20 times larger due to the presence of leakier inner tubes and the close spectral proximity of the resonant edge of t_1 and t_2. Although the design of Fig. 10 shows a narrower bandwidth than the first band design (Fig. 9), it presents some additional benefits, such as a lower minimum and polarization dependent loss, and likely greater mechanical robustness because of its thicker tubes.

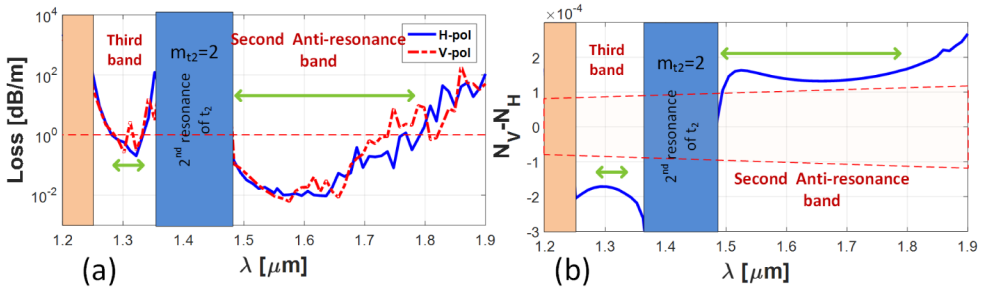

Fig. 10. (a) Loss and (b) birefringence of the optimized new proposed design with thicker tubes at λ_0 = 1.55µm with R = 7µm, Z = 0.65R, d = 1.5µm, $t_1 = t_{22}$ = 1.172µm and t_2 = 1.42µm. The fiber shows a large bandwidth (~300nm) PMB = ~1.45×10^{-4} with a loss < 1dB/m.

4. Single polarization designs

In addition to PMB, some applications like ultra-sensitive sensing or gyroscopes, or ultra-high power single polarization laser delivery may require a large polarization extinction ratio. The large birefringence in the fiber designs proposed so far decreases the beat length and reduces the possibility of coupling between polarization modes, which allows the input polarization state to be maintained. Here, we propose a modification to our polarization maintaining Hi-Bi NANF to provide both PMB and a large polarization extinction ratio, which transforms it into a polarizing fiber. The new structure not only has the favorable Hi-Bi characteristic but also shows a very large polarization differential loss (PDL) that can remove the unwanted

Optics EXPRESS

polarization component of the input light, as well as limiting distributed inter-polarization coupling due to surface roughness and micro-bends [34].

Our modification is based on a well-known method used to strip higher order modes from a few moded fiber [39, 40], which we have adapted to achieve "polarization dependent mode stripping". In this method, we selectively couple a specific polarization of the fundamental core mode into a lossy cladding mode, while the orthogonal polarization experiences almost no change. Here, the two main structural features of the former proposed 4-tube NANF are fundamental.

First, the induced large birefringence in the fiber creates an opportunity to clearly separate the effective index of the two polarizations, of which only one is index matched and out-coupled to lossier cladding (i.e. guided inside the tubes) modes. Based on the similarity of the guidance mechanism in NANFs and in simpler hollow core fibers made of a borehole in glass, it is possible to calculate the necessary geometrical specifications to match the index of the core and cladding modes [41]. The effective index (N_{eff}) of the FM in a single tube can be calculated with the following exact equation [42]:

$$N_{eff} = \sqrt{1 - \left(\frac{u_0}{R.K_0}\right)^2}. \qquad (3)$$

where $K_0 = 2\pi/\lambda$, R is the core radius and u_0 is similar to Eq. (1). As it is clear from this equation, the effective index is related to the size of the tube. Therefore, in order to have index matching between the core mode and one of the peripheral tubes in a NANF, they must have approximately the same size.

Here, the second useful feature of the 4-tube NANF is the very large size of the nested tubes. This allows the described mode matching to be engineered in the design. In fibers with more than four nested tubes, although the cladding tubes are large enough to strip the higher order modes [30, 39, 40], they are too small to enable fundamental mode out-stripping. Following this idea, we modified the radius of two opposite inner clad tubes in order to introduce index matching to the polarization with the highest loss in the Hi-Bi NANF of Fig. 8.

Figure 11 shows the structure and mode profiles of both high and low loss polarizations of the proposed polarizing NANF (P-NANF). The modified nested structure with a different distance (Z_1) between the two innermost rings in the vertical direction opens up a matching window for vertical polarization to couple to the cladding mode. Consequently, vertically polarized light leaks through the outer tube. This does not occur for the light on the Horizontal polarization, Figs. 10(b) and (c).

Figure 12 shows the simulated PMB, the loss of each polarization and the loss ratio between the two polarization for a fiber with R = 7µm, Z = 0.65R, Z_1 = 1.74R, d = 1.5µm, t_1 = 1.172µm, and t_2 = 1.42µm that has been designed for operation around λ_0 = 1.55µm. Here, we plot the polarization loss ratio (PLR) factor instead of the polarization dependent loss (PDL) as the ratio can provide a better measure of the effectiveness of the polarization stripping effect.

Optics EXPRESS

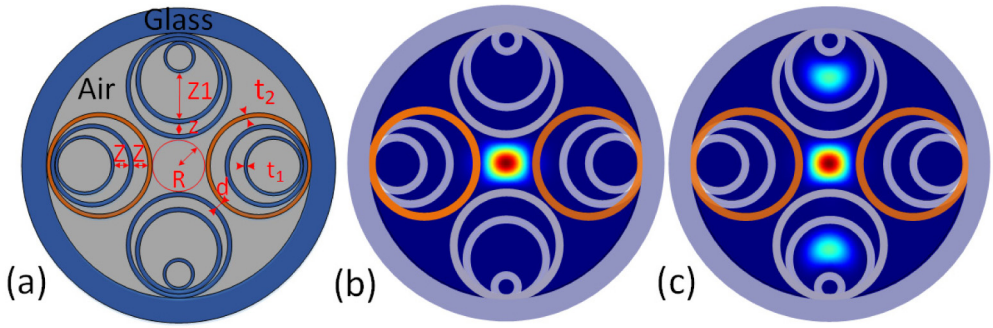

Fig. 11. (a) The proposed structure for polarizing NANF (P-NANF) and its (b) low loss polarization (horizontal), and its (c) high loss polarization (vertical). The coupled field to the cladding tubes in the vertical polarization increases the loss significantly.

The modified design shows a relatively large bandwidth of ~100nm with an almost constant PMB of ~1.5×10^{-4}. The loss of the low loss polarization is less than 1dB/m and the design exhibits a PLR of about 1000 at the wavelength of 1.55µm. A polarizing window of ~10nm with PLR>100 can completely eliminate any undesirable cross-coupled polarization over a sufficiently long propagation distance. The fiber can therefore provide an almost pure polarized output, regardless of the input polarization state, which may have applications in, manufacturing and machining as well as in high precision gyroscopes that require modes with relatively pure linear-polarization.

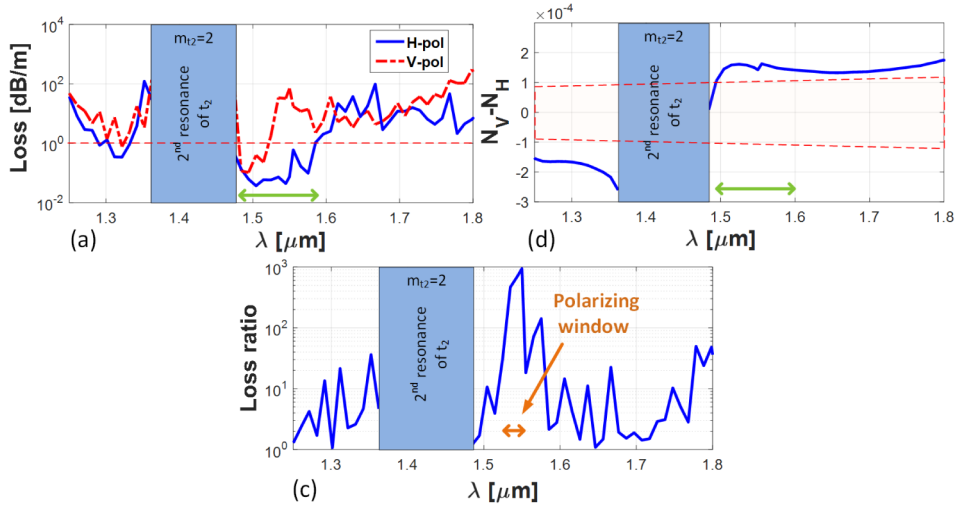

Fig. 12. (a) PMB, (b) loss and (c) PLR (High-loss/Low-loss) of the optimized P-NANF at λ_0 = 1.55µm with R = 7µm, Z = 0.65R, Z_1 = 1.74R, d = 1.5µm, t_1 = 1.172µm and t_2 = 1.42µm. The fiber has a bandwidth of ~100nm with PMB~1.5×10^{-4} and loss of the low-loss polarization <1dB/m. The PLR at λ_0 = 1.55µm is 1000 which gives the fiber a strong polarizing property.

5. Conclusions and discussion

In summary, we have presented a detailed study of various ways to obtain broadband polarization maintaining capability in antiresonant hollow core fibers, in particular for the NANF structure. We showed that achieving birefringence through asymmetric core designs adopted following the form-birefringence strategy in solid-core PM fibers is not effective in ARFs. Next, we adopted a different strategy, used in birefringent PBG fibers, where we broke the geometrical symmetry of a 4-tube NANF by introducing a bi-thickness design. To study the induced birefringence in this design, we introduced a decomposition analysis through

Optics EXPRESS

which we showed the thickness of tubes along the horizontal and vertical directions control, almost independently, the properties of the two respective polarizations. This approach provides a better understanding of the role of the individual thickness parameters in this structure as well as a method for practical fiber design.

Using the developed method, we identified a region with potential for ultra-broadband high birefringence within the first antiresonant window of a bi-thickness NANF. By proposing a radical design, we showed that the loss in this region can be mitigated, despite the small core size necessary for large birefringence. Our design not only offers a high birefringence ultra-broadband spectral window ~550nm (that is almost 6 times boarder than ever reported in a birefringent HC-ARF [33]) with birefringence as large as 1.5×10^{-4} and a loss of less than 1dB/m, but it also allows for losses as low as 0.04dB/m at a wavelength of 1.55μm. In addition, by sacrificing some bandwidth we proposed an alternative design with thicker tubes operating in the second anti-resonance band that achieves an order of magnitude lower loss (0.004dB/m at the wavelength of 1.57μm) and a large bandwidth (~300nm).

In order to add a polarizing effect into the design, we introduced a new polarization dependent mode stripping mechanism into the proposed bi-thickness NANF structure. The P-NANF structure offers a polarization dependent loss ratio of 30dB at the operating wavelength of 1.55μm with a minimum loss of 0.076dB/m and a low loss bandwidth of 100nm. With such a high loss ratio, the fiber can act as a polarizer for any unpolarized input over only a few meter of propagation, which would be of interest in applications requiring extremely high polarization extinction ratio.

Although the proposed fibers have been designed and optimized to operate in the telecommunication wavelength bands (i.e. around 1.55μm), the geometrical scalability of ARFs with the operating wavelength allows a straightforward application of similar design scenarios to other wavelengths more relevant to other applications, e.g. 1 μm for high power laser delivery or visible wavelengths for biomedical nonlinear endoscopy.

Funding

UK EPSRC through grants EP/I01196X/1 (HYPER-HIGHWAY).

Acknowledgments

FP and DJR gratefully acknowledge financial support from the UK Royal Society. The data for plots in this paper can be found at http://dx.doi.org/10.5258/SOTON/397073.